

# Growing solid deuterium for UCN production

Ekaterina Korobkina <sup>a,b,c,\*</sup>, Igor Berkutov <sup>b,c</sup>, Robert Golub <sup>b,c</sup>, Paul Huffman <sup>b,c</sup>, Clark Hickman <sup>b,c</sup>, Kent Leung <sup>b,c,d</sup>, Graham Medlin <sup>b,c</sup>, Matthew J. Morano <sup>b,c</sup>, Thomas Rao <sup>b,c</sup>, Cole Teander <sup>b,c</sup>, Christian White <sup>b,c</sup> and Albert R. Young <sup>b,c</sup>

<sup>a</sup> Department of Nuclear Engineering, NC State University, NC, USA

E-mail: [ekorobk@ncsu.edu](mailto:ekorobk@ncsu.edu)

<sup>b</sup> Department of Physics, NC State University, NC, USA

<sup>c</sup> Triangle Universities Nuclear Laboratory, Durham, NC, USA

<sup>d</sup> Department of Physics and Astronomy, Montclair State University, NJ, USA

**Abstract.** We have experimentally studied growing a large (about 1 liter) ortho-deuterium crystal in a real UCN source cryostat and recorded the growing process optically using a camera. The best quality was observed when growing the crystal directly from a vapor phase. The crystal was grown at different mass flows of deuterium and annealed at different temperatures. Optimum conditions were found for both, obtaining an optically transparent crystal and cooling it down with minimal damage. We found that the quality, final shape and changes during annealing of the crystal are very much dependent on the temperature profile of the cryostat walls.

Keywords: Solid deuterium, ultra-cold neutrons

## 1. Introduction

Deuterium is one of the best slow-neutron source materials due to its effective moderating properties and low absorption cross section [23]. It is intensively used for the production of cold neutrons (CN) [1,7,9] and ultra-cold neutrons (UCN) [4,11,12,25,31] and is proposed to be used for very cold neutron (VCN) sources as well [2]. Nevertheless, there is a distinctive difference between CN and UCN sources: the former use liquid deuterium, while latter benefit tremendously from increased UCN production cross section of solid deuterium [24]. The caveat is that the internal structure of solid deuterium crystal can affect significantly the neutron yield by decreasing it below theoretically predicted value.

In general, this is related to the fact that the lower the neutron energy, the higher probability of losses and shorter the absorption length. Indeed, the absorption length,  $L_a$ , for CN is in the 100 m range and for VCN in the 10 m range, which is much larger than the typical neutron path in the source and neutrons can escape from the source without being lost. Now, if one looks at the UCN sources this is not the case: here  $L_a$  decreases to a few cm, which is smaller or comparable to the dimensions of the solid deuterium crystal itself.

Another difference between CN and UCN sources is their figures of merit: for cold neutrons it is usually integral neutron flux or brightness, while for UCN sources in most cases it is the neutron density  $N_{\text{UCN}}$ , which under steady-state conditions is a product of UCN production rate  $P$  and neutron survival time  $\tau$  in the source  $N_{\text{UCN}} = P\tau$ . In the ideal case of negligible other losses (discussed in the next section), the survival time in deuterium is  $\tau = L_a/v$ , where  $v$  is neutron velocity. Therefore, neutron survival and escape probability critically depend on the distance

---

\*Corresponding author. E-mail: [ekorobk@ncsu.edu](mailto:ekorobk@ncsu.edu).

$L$  traveled inside the deuterium bulk: only if  $L < L_a$  the neutron has a significant chance to leave the source. A deuterium layer for production of extractable UCN should therefore be thinner than  $L_a$  calculated with the maximum UCN velocity.

To estimate the UCN density in the experiment,  $N_{\text{exp}}$ , we also have to account for the transmission probability from the deuterium bulk to the experimental set-up,  $T_{\text{exp}}$ , which is proportional to the probabilities of transmissions through the bulk,  $T_{\text{bulk}}$ , the top layer of the crystal,  $T_{\text{top}}$ , and transport through the neutron guide,  $T_{\text{guide}}$ , i.e.,  $N_{\text{exp}} = P\tau T_{\text{bulk}}T_{\text{top}}T_{\text{guide}}$ . Elastic scattering on imperfections and grain boundaries in the bulk increases travel inside the bulk and reduces  $T_{\text{bulk}}$  (see a comprehensive discussion and simulations about the bulk transmission in [22]), while imperfections of the deuterium/vacuum boundary decrease  $T_{\text{top}}$  [3]. Therefore, to achieve ultimate density it is imperative to know how to grow crystals with good quality of both the bulk and surface. One easily accessible evidence of good crystal quality is its optical transparency/opacity. While an optically transparent crystal still can be mosaic and increase  $L$  due to elastic scattering on some density fluctuations compatible with the UCN wavelength, the opaque crystal with visible numerous imperfections was experimentally confirmed to have worst transmission [13]. In the present publication we report results of our visual monitoring of solid deuterium crystals grown in the real UCN source cryostat under different conditions relevant to operation of UCN sources.

## 2. Solid deuterium properties related to ultra-cold neutron production

In this section we will review several properties, important for understanding our results on growing a solid deuterium crystal ( $\text{SD}_2$ ).  $\text{SD}_2$  is a quantum molecular crystal with a weak intermolecular interaction and a large zero point energy. Its properties have been well studied, see for instance the review of Silvera [26]. First we need to mention a strong temperature activated diffusion above 9 K, where diffusion activation energy is  $E_D/k_B = 290$  K [26,30]. The diffusion coefficient  $D = D_0 \exp(-E_D/k_B T)$ , where  $D_0 = 2.3 \times 10^{-3} \text{cm}^2/\text{s}$ , changes 7 orders of magnitude between 9 K, and the triple point  $T_{\text{triple}} = 18.7$  K. Due to such high mobility it is possible to grow quite good quality single crystals near the triple point. The problem is that most experiments require much lower temperatures and during cooling cracking can happen, leading to degraded quality. The cracking is the result of a strong temperature dependence of the molar volume, which changes from  $20.4 \text{cm}^3/\text{mol}$  at  $T_{\text{triple}}$  down to  $19.95 \text{cm}^3/\text{mol}$  at 10 K as shown in Fig. 1(a) [17]. Nevertheless, it turns out that  $\text{SD}_2$  demonstrates the so-called ‘‘triple wetting’’ phenomenon, which means that above  $T_{\text{triple}}$  a film of  $\text{D}_2$  molecules can be of infinite thickness, while below  $T_{\text{triple}}$  wetting coefficient exponentially drops (Fig. 1(c), [28]) and only a few monolayers thick film can stick to the surface of the container, while the bulk is growing as islands of  $\text{SD}_2$  crystals. In other words, below  $T_{\text{triple}}$  deuterium molecules prefer to stick to themselves. This property can help in successful cooling of  $\text{SD}_2$  crystals by annealing long enough to allow  $\text{SD}_2$  to move off the walls.

In connection with UCN production, we also need to mention that only the ortho-deuterium spin species must be used to avoid additional losses. Indeed, ultra-cold neutrons are produced not by the moderation process, which results in thermal equilibrium of neutrons with the moderator. UCN in  $\text{SD}_2$  are converted from higher energies (cold neutrons) to neV range by a single down-scattering and are not in thermal equilibrium with the deuterium converter. Therefore, upon secondary interaction with  $\text{SD}_2$ , UCN can gain energy and turn back into a cold/thermal neutron. There are two possible up-scattering processes: absorption of a phonon or a spin flip. The latter converts the para-deuterium (corresponding to the lowest rotational band with odd rotational spin  $J = 1$ ) to lowest ortho-state with even  $J = 0$  [19]. Phonon density can be reduced enough to be neglected by cooling the crystal below 5 K, while the spin flip cross section is temperature independent and can be only suppressed by reducing the para concentration below 1%. In addition, the concentration of HD molecules also should be kept well below 1% to avoid losses due to absorption and upscattering on hydrogen (hydrogen  $\sigma_a = 0.3263$  barn, deuterium  $\sigma_a = 0.000519$  barn).

Important thermodynamic properties of  $\text{SD}_2$  are the saturation pressure and thermal conductivity shown in Fig. 1(b) and (d), respectively [16,29]. Note that the saturated pressure was measured in [29] for ‘‘normal’’ deuterium, which is an equilibrium concentration of para and ortho molecules at room temperature. In [6] a difference in the saturation pressure between ortho and para species was studied down to 15 K and ortho pressure was found

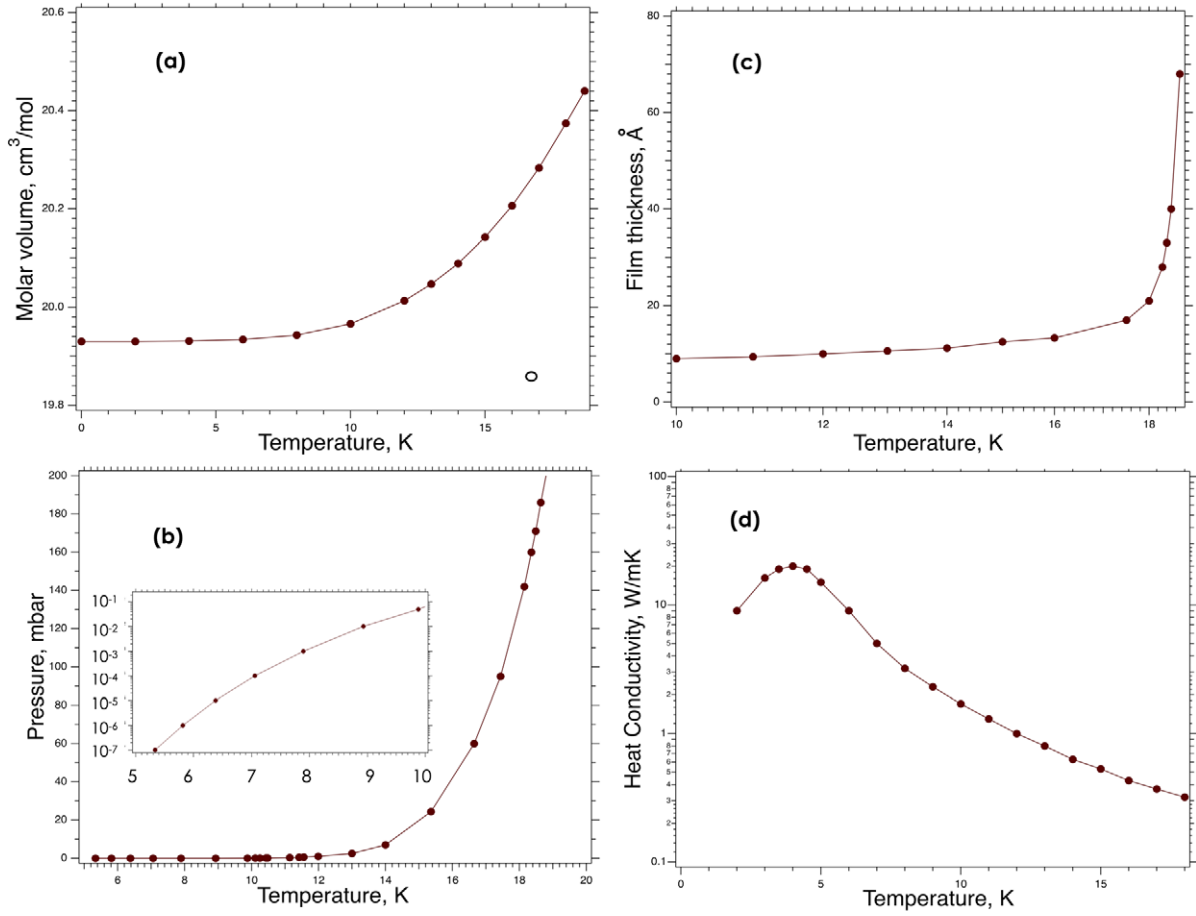


Fig. 1. Temperature dependent properties of solid deuterium below the triple point: (a) – molar volume; (b) – saturated pressure; the insert shows it (also in mbar) below 10 K on a logarithmic scale; (c) – film thickness; (d) – heat conductivity.

to be only about 6% higher, which is not reflected in Fig. 1(b), because what we want to emphasize here is that the saturation pressure, similar to the diffusion coefficient and molar volume is rising noticeably only above 10 K [29]. In contrary to the weak pressure dependence, the thermal conductivity and heat capacity can change quite dramatically [10] depending on the relative concentration of ortho- and para-fraction. The thermal conductivity has a maximum at around 4 K, while dropping 2 orders of magnitude near the triple point. Such behavior means that above 4 K if there is a temperature gradient in SD<sub>2</sub>, the hot layer will be rather small and the crystal would mostly be cold.

### 3. Experimental setup overview

For optical Raman studies small single hydrogen crystals of several cm<sup>3</sup> size have been successfully grown from vapor at  $0.7T_{\text{triple}}$  temperature to avoid cracking [26] (for deuterium  $0.7T_{\text{triple}} = 13$  K).  $0.7T_{\text{triple}}$  was chosen empirically, considering that there is almost no more change in the molar volume below this temperature, while there is still some mobility due to non-negligible saturation pressure and non-zero diffusion (see Fig. 1). The crystals were grown up to 11.5 cm length in small cylindrical cells of 1 cm diameter, in a well controlled temperature environment. Crystal growth started from walls and only in the center there were some imperfections. Slightly larger

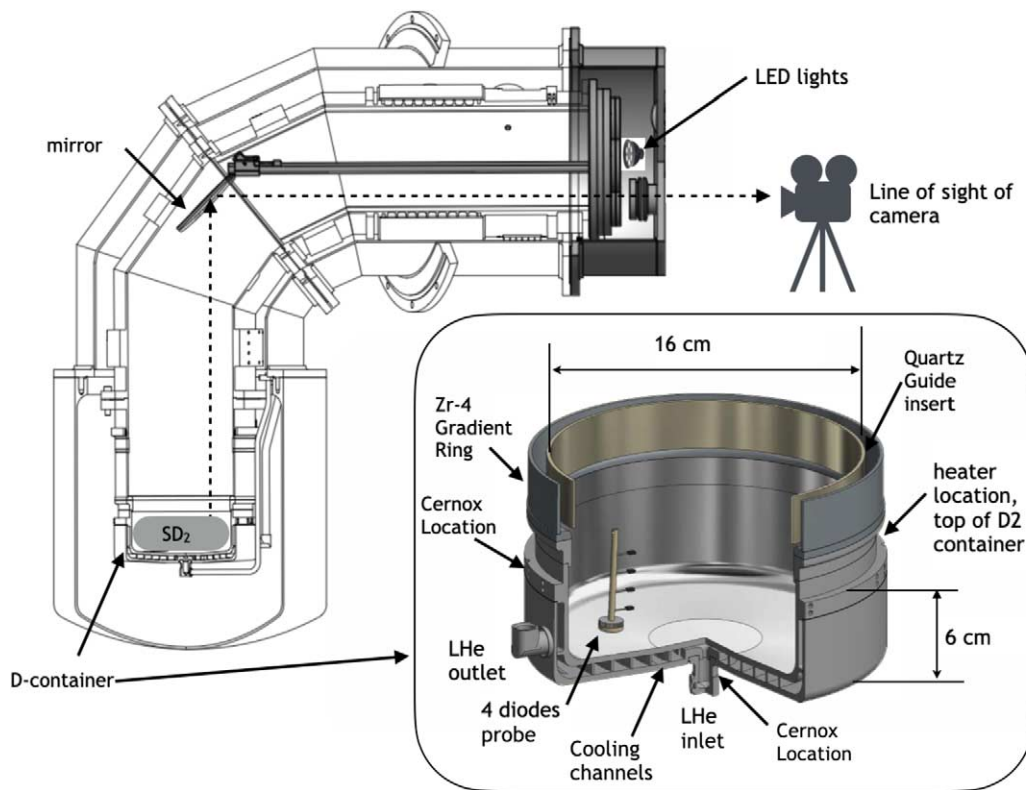


Fig. 2. Cross-sectional view of the experimental set-up: the camera was located outside the vacuum jacket; a warm optical window was mounted on the vacuum jacket, another one on the cold cryostat flange; LED light source was mounted inside the vacuum jacket; a mirror with an adjustable angle was located inside the inner vacuum. Deuterium was solidified in the D-container at the bottom part of the cryostat. The insert shows a 3D-rendering of the D-container including locations of the instrumentation: a heater made of NiCr wire; two Cernox temperature sensors, one located at the LHe inlet, another just below the heater on the outer wall of the container; a holder made of PEEK with 4 calibrated diodes ( lakeshore, DT-670-SD ) separated vertically by 1 cm and positioned inside the container to probe temperatures directly inside the  $\text{SD}_2$  bulk.

sample cells with optical windows were used in [5,8] and in studies of  $\text{SD}_2$  growing from liquid and vapor phases [21], for studies with cold and ultra-cold neutrons with different degrees of success. Such geometries have an essential difference from a real UCN source, with its much larger  $\text{SD}_2$  volume, unavoidable temperature gradients in the container walls, and a large open top surface of  $\text{SD}_2$  needed for UCN extraction. As the present study has revealed, these differences do matter. Therefore, for a successful operation of a UCN source it is important to do tests in the real source cryostat.

The overall design of the PULSTAR UCN source is described in [15]. The source is designed to be installed inside the former thermal column of the reactor. Nevertheless, flexibility of the helium transfer lines allowed us to assemble the source cryostat outside the biological shield and test the growing of  $\text{SD}_2$  in situ. The experimental layout is shown in Fig. 2. Since the cryostat has an elbow shape, a “dentist mirror” setup was used to observe the bottom part of the elbow, called D-container, where the  $\text{SD}_2$  condensed [20]. The D-container has double walls with cooling channels, which distributed cold He flow from inlet all around the bottom plate. Depending on the required temperature of the cryostat, either cold He gas or two-phase flow was delivered to the He inlet through 6 mm O.D. tubing. The cold flow was returned back to the liquefier through an exhaust outlet at the side wall of the D-container. The O.D. of tubing connecting the outlet to the liquefier is gradually increasing from 9.5 mm to 12.5 mm to avoid LHe flow oscillations. The container was made from Al6061 alloy and electron beam welded to the neutron guide elbow above through a so-called “gradient ring” made of Zr-4 alloy explosively bonded

to Al6061. Since Zr-4 has a much smaller thermal conductivity than Al6061, the ring thermally decoupled the D-container from the neutron guide elbow to allow for about 20 K temperature gradient. This design prevented deuterium condensation on the neutron guide wall of the elbow.

To monitor temperatures, there were three Cernox sensors located at the inlet (one sensor) and at the top of the container just below the gradient ring (two sensors). The temperature of the exhaust helium was measured by a diode located in the LHe transfer line about 3 meters away. In addition, specially for the present test a plastic holder with four calibrated diodes (Lakeshore, DT-670-SD) was positioned inside the D-container to probe temperatures directly inside the deuterium. The diodes were separated vertically by 1 cm and are labeled by their distance from the bottom of the container as 1 cm, 2 cm, 3 cm and 4 cm. These diodes were providing temperatures in the bulk, while surface temperature (when not condensing) was characterized by gas independent pressure gauges. To control the cryostat temperature and to facilitate melting and evaporation, a heater made from NiCr wire was placed in the groove just below the gradient Zr-4 ring.

#### 4. Growing solid deuterium at different temperatures

We have studied  $\text{SD}_2$  condensation under different thermal conditions, which can be summarized as “low temperature range” (deposition at operational temperature of UCN source around 6 K), “high temperature range” (above 14 K, i.e., close to triple point) and “intermediate temperature range” (12 K–9 K). As one can see below, the crystal bulk is very different in quality. In addition, our study revealed a problem of surface frost formation during cooling and accidental temperature instabilities.

##### 4.1. Low temperature range

The low-temperature deuterium deposition was motivated by the Mainz UCN source mode of operation [27]. This facility has a horizontal geometry of the cryostat and can deposit deuterium only from vapor at an operational temperature of the source around 7 K. The Mainz team had tested different deuterium flow modes, verifying crystal quality by the observed UCN yield but without optical control [18]. The best results were obtained with a “slow deposition” rate of about  $< 3$  mm/h at a flow rate of about 0.3 stl/min. In our setup, the goal was to verify the optical crystal quality at similar conditions. The first deposition was made at a  $\text{D}_2$  pressure of 10 mbar and a flow rate of 0.3 l/min. As can be seen in Fig. 3(a) and (b), the deuterium does not cover the container with a smooth layer. It rather grows as 3D crystallites (looking very similar to water hoarfrost), which are slowly merging with each other. This is a direct consequence of the triple-point wetting feature of solid deuterium. In Fig. 3(b) one can also notice that there are more holes near the walls. We have not used the heater in this run, but the walls are warmer because of the heat leak from the elbow and obviously, deuterium condenses preferably toward the center. An interesting observation was that a crystallite layer growing on the walls was bending and falling down to the bottom (a ring near the walls in Fig. 3(b)). Nevertheless, the crystallites themselves look dense. On the other hand in Fig. 3(c), one can see fluffy snowflakes, which are the result of a high flow rate of  $> 2$  l/min and a maximum  $\text{D}_2$  pressure of 250 mbar for about 25 min. At the end of the condensation the crystal height was about 3 cm (the diode labeled as 3 cm was just covered). Interestingly, this was the only run where a gradient of about 0.5 K was observed between readings of the embedded diodes. In all following runs the temperature difference was below 0.1 K after the end of condensation.

After deposition, the crystal was annealed using heaters at 12 K (top of D-container) overnight, which resulted in the merging of hoarfrost into a bulk of a few mm sized, rather transparent than opaque crystallites. The embedded diodes were showing 8.75 K (1 cm), 9.5 K (2 cm) and 10 K (3 cm) right after the heater was switched on and slowly cooling and approaching each other throughout the annealing process. After 15 hours of annealing the readings were 7.25 K (1 cm), 7.75 K (2 cm) and 8.75 K (3 cm), which is the result of improved thermal conductivity due to formation of larger grains. After this intermediate annealing we tested the deposition at increased flow rates, using 0.1 l/min step increments. At a flow rate of about 0.8 l/min the newly deposited layer became transparent and at

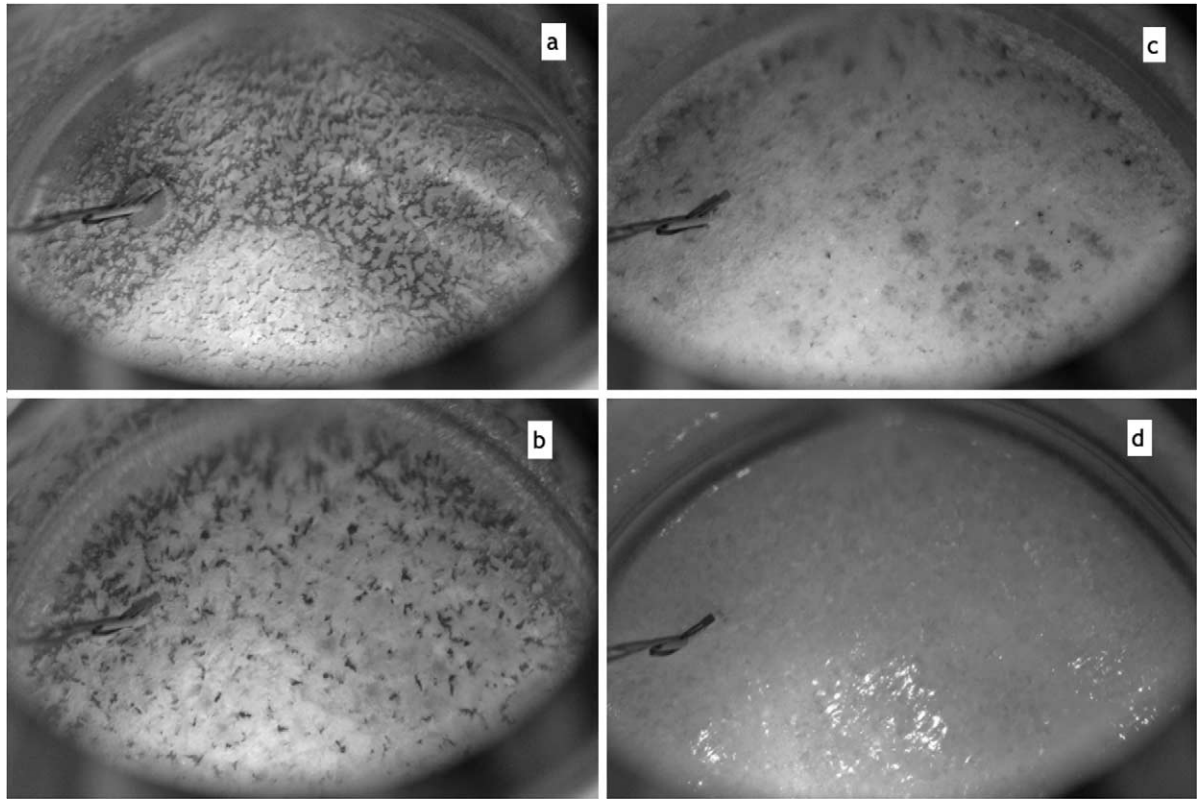


Fig. 3. Crystal growth in the low-temperature range. (a) – and (b) – different stages of condensation at deuterium flow of 0.3 l/min, (c) – after accidental  $D_2$  flow increased over 2 l/min for 15 min, (d) – crystal annealed at 12 K overnight at  $D_2$  flow of 1.2 l/min.

1.2 l/min the surface became very shiny (see Fig. 3(d)). The conclusion is that such flows facilitate the increase of  $SD_2$  surface temperature close to the triple point, producing a “polishing effect” in the thin top layer. As was mentioned above, due to the thermal conductivity rising towards 4 K, such a layer would be rather thin. Indeed, the embedded diodes showed temperatures below 13.2 K, 12.5 and 11.5 K for 3 cm, 2 cm and 1 cm respectively. After the deuterium flow was stopped, the gradient between the diodes at 2 cm and 3 cm became  $< 0.2$  K, while between the diodes at 1 cm and 2 cm it was still 0.5 K meaning that such high flows had an annealing effect on the top of the crystal, while the bottom was still rather heterogeneous. As a result of the flow study, the conclusion was drawn that in our setup the flow should be  $\geq 0.8$  l/min to produce a transparent crystal. Such flow rates were used in all our consecutive runs.

#### 4.2. High temperature range

Our temperature reconstruction shows that the optimum temperature range to produce transparent crystals corresponds to the coldest cryostat spot temperature,  $T_{\text{cold}} \geq 12$  K, which is consistent with the  $0.7T_{\text{triple}}$  rule. The beginning of crystal growth at  $T_{\text{cold}} = 14$  K is shown in Fig. 4(a) and (b). The crystal looks absolutely transparent. The deuterium flow was 0.8 l/min, helium inlet was at  $T_{\text{inlet}} = 8$  K, helium outlet  $T_{\text{outlet}} = 17.5$  K, and top of the container was at  $T_{\text{top}} = 17.5$  K. This was our first high-temperature run, when we were just learning how to control the temperature. In this particular run the increased temperature was obtained by reducing the cooling He flow. At one moment the flow was interrupted and deuterium was quickly evaporated and then re-deposited. As one can see on Fig. 4(c), fast re-condensation has not produced a good crystal even at such high temperatures. Therefore, both conditions of optimum flow and temperatures must be fulfilled for a good result.

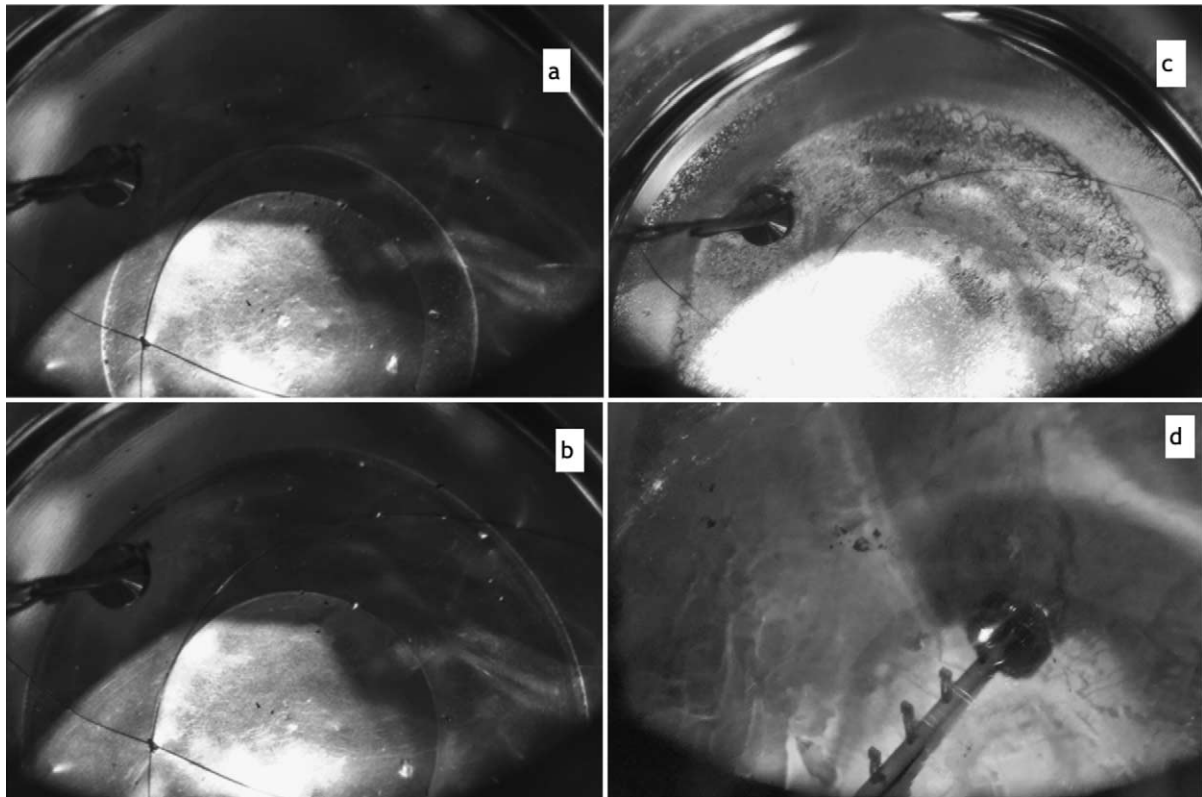


Fig. 4. Deuterium condensation at high temperature range: (a) and (b) – transparent crystal growing at  $T_{\text{inlet}} = 8$  K,  $T_{\text{top}} = 17.5$  K,  $T_{\text{outlet}} = 17.5$  K, (c) – crystal re-condensed after accidental fast evaporation, (d) – another run, crystal is grown initially at  $T_{\text{inlet}} = 7$  K,  $T_{\text{top}} = 15.8$  K,  $T_{\text{outlet}} = 16.5$  K with deuterium flow of 1.3 l/min gradually slowing down to 0.7 l/min, full inventory condensed.

Later we improved our technique of successful high-temperature runs. An example of condensation of an about  $1000 \text{ cm}^3$  large crystal is shown in Fig. 4(d). This condensation was made without the use of heaters to avoid temperature gradients (see Section 5). Instead, we regulated the He flow down to keep the container at the initial temperature of 9 K (measured by the pressure of residual  $\text{D}_2$  film before opening the  $\text{D}_2$  flow). After starting deuterium flow, the helium inlet was at  $T_{\text{inlet}} = 7.5$  K, helium outlet  $T_{\text{outlet}} = 16.3$  K, and top of the container was at  $T_{\text{top}} = 15.8$  K. The initial deuterium flow was 1.3 l/min to use the heat of condensation to keep the top layer warm enough for self-annealing. The flow was gradually reduced toward the end of condensation (because of reduced pressure in the storage tank) to let the crystal cool naturally to 13 K over several hours. This strategy worked best for our set-up and was adopted as a procedure to grow deuterium for future runs with UCN.

#### 4.3. Intermediate temperature range

Condensation in the intermediate temperature range was done using a combination of a high cooling flow and a high power of D-container heaters in an attempt to warm up the walls of the container to the conditions similar to the run shown in Fig. 4(a) and (b). The top of the container was at 16 K,  $T_{\text{inlet}}$  was at 7.5 K, but the He outlet temperature was only 13 K compared to 17.5 K for the high-temperature run. Different stages of condensation are shown on Fig. 5, with (c) showing about  $350 \text{ cm}^3$  condensed volume and (d) corresponding to the end of condensation of about  $800 \text{ cm}^3$ .

The crystal grown in the intermediate temperature range looks different from those obtained in the low- and high-temperature runs. In the middle, the crystal looks semi-transparent at the beginning (Fig. 5(a)). Then the

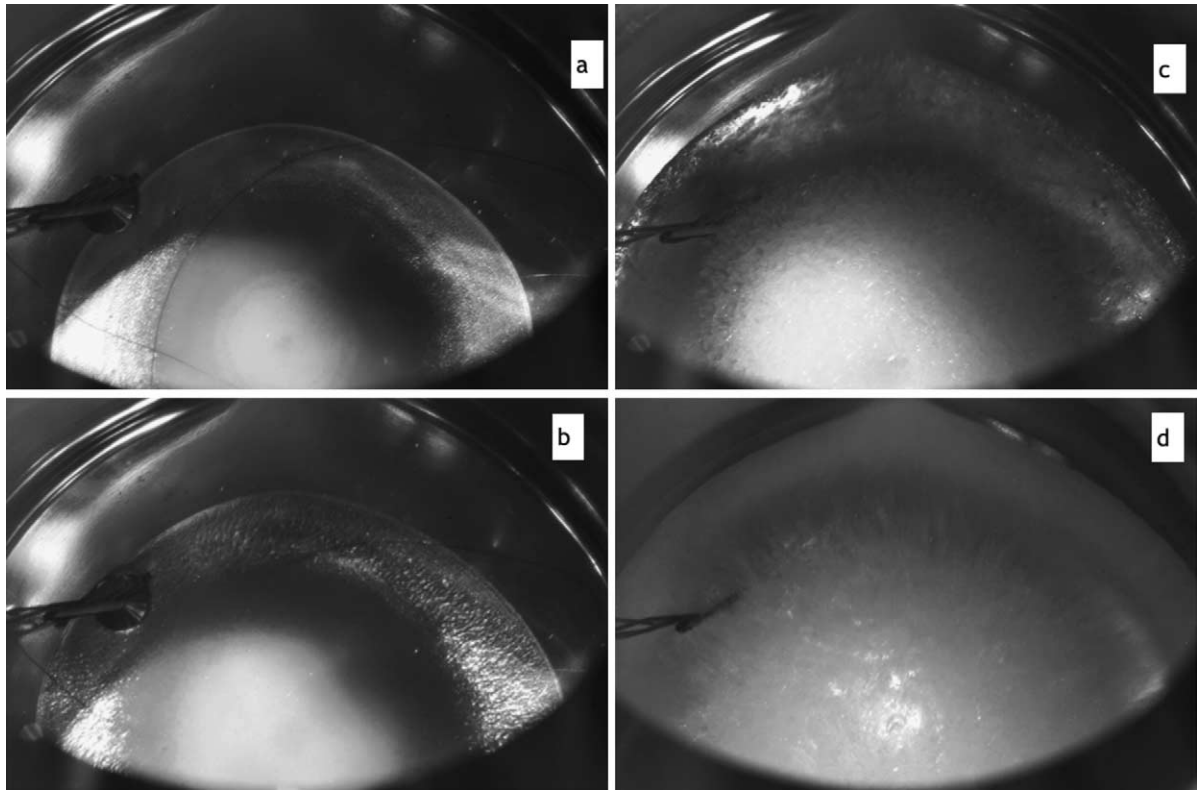


Fig. 5. Deuterium condensation at intermediate temperature range: (a) and (b) – 5 min and 50 min after the start of condensation; (c) – 350 cm<sup>3</sup> of SD<sub>2</sub> condensed; (d) – about 800 cm<sup>3</sup> of SD<sub>2</sub> condensed.

center transforms to small crystallite-like bulk (surrounded by a semitransparent halo) (Fig. 5(b)), with grains gradually growing in size, as visible through Fig. 5(c) toward Fig. 5(d). The structure of the latter looks similar to the annealed version of the low-temperature crystal shown in Fig. 3(d). A peculiarity of this run is the fact that even an 800 cm<sup>3</sup> crystal does not cover the entire bottom of the container. Another peculiarity is that the embedded diodes were covered later, and only after a larger deuterium mass had flown to the cryostat than in any other run. The explanation of both peculiarities requires a better understanding of the effect of a large thermal gradient on the crystal shape, as described in the next section.

## 5. Effect of temperature gradients on crystal shapes

A temperature gradient along the walls of the cryostat can affect the crystal, especially in geometries with a large free surface. As was described in the Section 2, solid-deuterium properties are strongly temperature dependent above 10 K. The consequences are somewhat different for deuterium condensation, depending on whether  $T_{\text{cold}}$  is below (“cold” gradient) or above 10 K (“warm” gradient).

The cold gradient was present in the condensation at intermediate temperature, described above in Section 4.3. Based on our temperature reconstruction during condensation (Fig. 6(c)), the  $T_{\text{cold}}$  for this run was 9.3 K and the temperature gradient between  $T_{\text{top}}$  and  $T_{\text{cold}}$ ,  $T_{\text{top}} - T_{\text{cold}} = 7.5$  K. Under such conditions the deuterium was freezing in the center of the cryostat, avoiding the warmer walls. The embedded 1 cm diode was showing about 12 K after it was covered with deuterium. As one can see from the image (c) of Fig. 5, only about 2 cm outwards of the diode was covered with a rather transparent and thin layer. Our approximations of the resulting shapes for

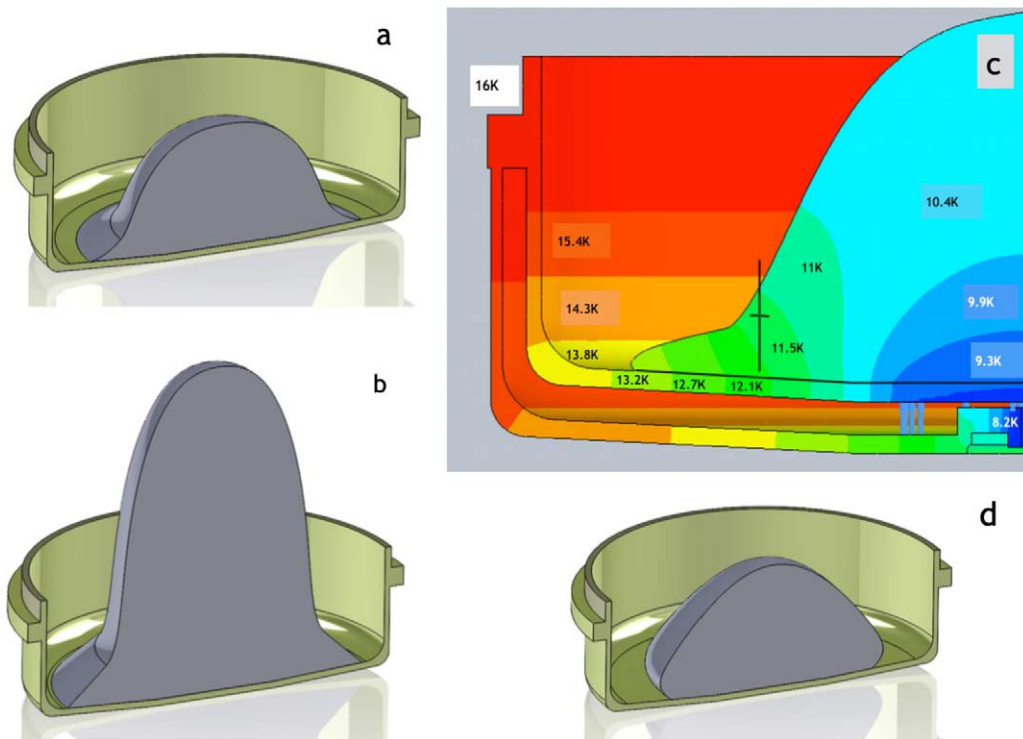


Fig. 6. Effect of temperature gradient on the shape of the crystal: (a) and (c) – shape and temperature reconstruction of 350 cm<sup>3</sup> condensed D<sub>2</sub> at cold-gradient conditions; (b) – shape reconstruction of 800 cm<sup>3</sup> condensed at cold-gradient conditions, (d) – crystal shape after overnight annealing under warm-gradient condition.

the 350 cm<sup>3</sup> and 800 cm<sup>3</sup> condensed volumes are shown in Fig. 6(a) and (b). The height of the crystal on image (b) is about 15 cm. Apparently, in this case deuterium was not covering the walls with a temperature above 13 K. This is different from the warm-gradient case, where deuterium covers the entire bottom during condensation. Nevertheless, the warm gradient does affect the shapes, although not so much during condensation.

The first observation of a warm-gradient effect was accidental, due to the schedule of the PULSTAR reactor, which operates only during the working office hours of the university, usually from 7 o'clock till 16:30. As a result, our first condensation runs were done in separate steps throughout several days. When the crystal condensation shown in Fig. 4(c) was stopped at 90 cm<sup>3</sup> and left overnight at 12.5 K, a completely different shape was observed in the morning. Another portion of 100 cm<sup>3</sup> was added and the crystal again left overnight at 12.5 K. The result is shown in Fig. 7(a). Due to the combination of evaporation – re-freezing (at 1 mbar), high diffusion at higher temperatures of the wall and the “triple wetting” properties, solid deuterium transformed itself into a ball shape, weakly connected only to the coldest spot in the middle of the container. It also avoided the diode holder.

Later we repeated such overnight annealing and recorded a movie, which can be seen here [14]. Three images from the movie are shown in Fig. 7(b), (c) and (d). Image (b) was taken near the end of condensation, when the crystal covered the entire bottom. Image (c) was taken only 3 hours later, but the thinning of edges was already quite visible. Image (d) was taken 11 hours later, when most of the deuterium had already moved to the middle. The last image in Fig. 7 looks similar to Fig. 5(b), with the thin film halo surrounding the blob in the middle, only the bulk quality of the middle is different – milky or transparent. Our shape reconstruction of the 190 cm<sup>3</sup> condensed sample after overnight annealing is shown in Fig. 6(d).

In any case, both warm and cold gradients need to be avoided to keep the crystal as flat as possible. Crystal deformations can affect the angular distribution of extracted UCN and potentially reduce the UCN yield of the source. Indeed, in the ideal case of a flat crystal, the emitted UCN trajectories are preferentially parallel to the

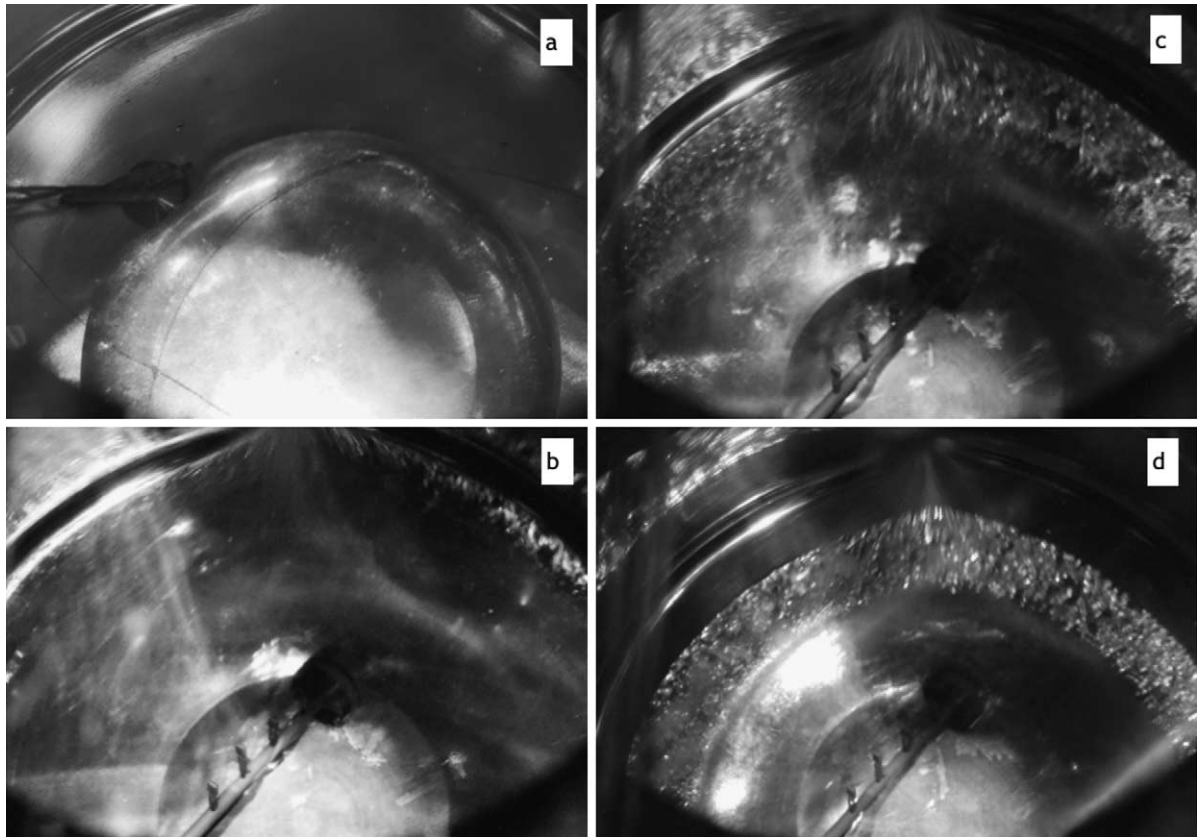


Fig. 7. Effect of temperature gradient on the shape of the crystal: (a) – crystal shape after overnight annealing at 12.1 K, 190 cm<sup>3</sup> of deuterium condensed, (b) – another run, right after deuterium flow stopped, (c) and (d) two intermediate stages of shrinking.

guide surface due to the kinetic energy gain along the normal to the crystal surface. Such focusing increases the extraction of high energy neutrons, while if the shape is more spherical, the effect of focusing disappears. Such a change of crystal shape might have caused the decrease of the slow VCN part of the spectrum at Mainz after annealing, described in [18]. In the extreme case of a columnar shape (as occurring in the cold gradient condensation), neutrons are accelerated towards the walls, which is the worst case.

## 6. Cooling down to operational temperature and the surface frost problem

In the section above it was described how to grow a transparent bulk crystal and avoid crystal shape deformations to facilitate good UCN transmission. Another effect, which strongly affects UCN yield even from a perfect crystal, is the quality of the crystal surface. The main culprit is a surface frost, which dramatically increases the probability of a neutron to be reflected back into the bulk of deuterium. In the present study the surface frost/facets formation of different degrees was observed during each cool-down when crystal temperature was approaching 11 K (see Fig. 8(a)). The faster it cooled down, the more facet/frost formation was visible. In the extreme case of very rapid cooling from  $T_{\text{triple}}$  to 14 K, the transparent crystal became completely black.

Only frost formation (no facets) was observed during accidental LHe flow instabilities and intentional “heat pulsing”. The result of an accidental slow LHe flow oscillation is visible as a dusty surface on the image in Fig. 8(c). In this case there were four warming-cooling cycles of approximately 30 min between crystal temperatures of 9.5 K

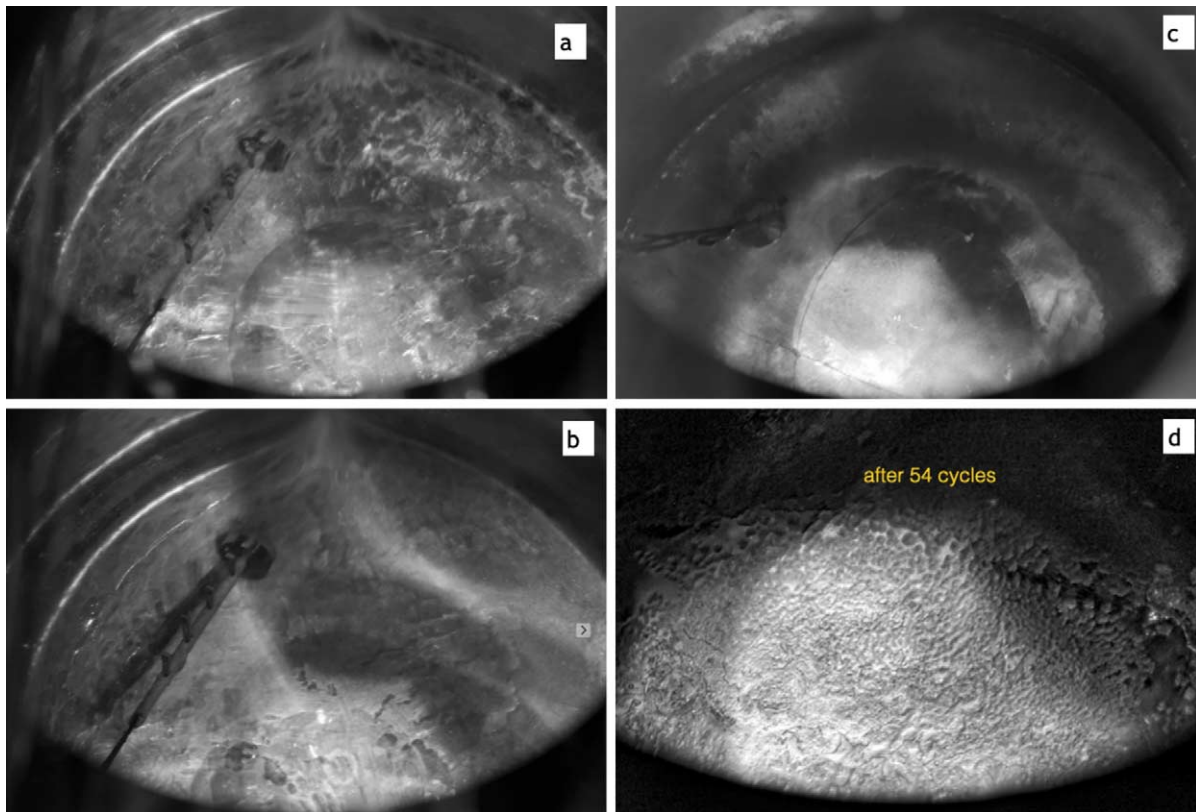


Fig. 8. Surface frost and facet formation: (a) – facets/frost formed during cool-down, when crystal temperature drops below 11 K; (b) – surface annealed by a 20 min temperature rise to at maximum 14 K due to a bubble in the LHe flow; (c) – surface dusted with a frost after LHe flow instability, crystal temperature was slowly oscillating 4 times between 9.5 K and 14 K during 2 hours; (d) – after 54 intentional heat pulses, crystal temperature was oscillating between 8.5 K and 9.7 K.

and 14 K. The frost here is not well visible, which is in contrast with the image in Fig. 8(d), where results of our following intentional pulsing are shown. In this run the temperature of the crystal was oscillating between the base 8.5 K and a maximum of 9.7 K. This first run of intentional pulsing is described in [3], where a problem of continuous slow decline of UCN yield at pulsed UCN sources was discussed in great detail, including simulations of the UCN yield versus frost thickness.

The crystal shown on Fig. 8(a) was also treated with the heat pulsing, but at lower temperatures. The base temperature was 7 K and the maximum was 8.4 K. No visible frost formation was observed in this case. The only effect was an accidental annealing of the surface by a 20 min temperature rise to the maximum 14 K due to a bubble in the LHe flow shown in Fig. 8(b). Later we were able to reproduce such annealing again, intentionally interrupting the LHe flow for a moment.

## 7. Conclusions and recommendation for design of solid-deuterium UCN sources at ESS

The main conclusion is that it is possible to grow a  $SD_2$  crystal of a good quality for UCN production. The quality and shape of the crystal are defined by the temperature profile of the cryostat walls. Therefore, when designing a UCN source one must take care about: (a) modeling of the thermal performance of the cryostat; (b) design the temperature sensor locations in such a way as to be able to characterize the temperature profile of the cryostat walls; (d) provide a cooling power sufficient to keep the  $SD_2$  temperature as close to 5 K as possible to avoid frost

formation; (e) design the LHe system in such a way as to avoid flow instability, minimize temperature gradients, and allow growing the crystal in the high temperature range. Special care must be taken about the surface frost formation. If possible, provide for testing of the crystal growth and surface annealing in the real cryostat before final installation.

The goal of the present study was to investigate and optimize growing of deuterium for the sources utilizing rather large  $SD_2$  crystals. Nevertheless, a different approach to UCN production was proposed a long time ago, which uses a thin film of solid deuterium [32]. Such a source can use a film of a 1 mm thick layer of  $SD_2$ . The main advantage is the possibility to accumulate UCN up to the saturation density, which does not depend on the geometry, volume or area of the source vessel. It is much easier to keep the thin film cold. An in-beam configuration can be rather transparent for cold neutrons (and allow the beam to be used by other experiments) and the practical realization can be quite simple. The shape of the source vessel can be easily adjusted even to a divergent neutron beam. While the intensity would be lower than that of a LHe source, it can be used as a test UCN source (similar to the test beam at the PF2 facility at ILL). The main cryogenic challenge would be to keep gradients at a very minimum to prevent film migration.

## Acknowledgements

The authors are grateful to the staff of the PULSTAR reactor, especially A. Cook, for the technical support. This work was supported in part by the US Department of Energy under grant number DE-FG02-97ER41042.

## References

- [1] P. Ageron, P. De Beaucourt, H.D. Harig, A. Lacaze and M. Livolant, Experimental and theoretical study of cold neutron sources of liquid hydrogen and liquid deuterium, *Cryogenics* **9** (1969), 42–50. doi:10.1016/0011-2275(69)90257-4.
- [2] A. Aleksenskii, M. Bleuel, A. Bosak, A. Dideikin, M. Dubois, E. Korobkina, E. Lychagin, A. Muzychka, G. Nekhaev, N. Nesvizhevsky, A. Nezvanov, R. Schweins, A. Strelkov, K. Turlybekuly, A. Vul' and K. Zhernenkov, Development of the very cold neutron source prototype, in: *28th International Seminar on Interaction of Neutrons with Nuclei*, May 24–28, 2021, <http://isinn.jinr.ru/past-isinns/isinn-28/presentations/26/Nezvanov.pdf>.
- [3] A. Anghel, T.L. Bailey, G. Bison, B. Blau, L.J. Broussard, S.M. Clayton, C. Cude-Woods, M. Daum, A. Hawari, N. Hild, P. Huffman, T.M. Ito, K. Kirch, E. Korobkina, B. Lauss, K. Leung, E.M. Lutz, M. Makela, G. Medlin, C.L. Morris, R.W. Pattie, D. Ries, A. Saunders, P. Schmidt-Wellenburg, V. Talanov, A.R. Young, B. Wehring, C. White, M. Wohlmuther and G. Zsigmond, Solid deuterium surface degradation at ultracold neutron sources, *Eur. Phys. J. A* **54** (2018), 1–15. doi:10.1140/epja/i2018-12594-2.
- [4] A. Anghel, G. Bison, B. Blau, M. Daum, N. Hild, K. Kirch, B. Lauss, D. Ries, P. Schmidt-Wellenburg, V. Talanov, M. Wohlmuther and G. Zsigmond, The ultracold neutron source at the Paul Scherrer Institute-performance and status, *J. Neutron Research* **20** (2018), 83–86. doi:10.3233/JNR-180086.
- [5] K. Bodek, B. van den Brandt, T. Bryś, M. Daum, P. Fierlinger, P. Geltenbort, M. Giersche, P. Hautle, R. Henneck, M. Kasprzak, K. Kirch, J.A. Konter, G. Kühne, M. Kuźniak, K. Mishima, A. Pichlmaier, D. Rätz, A. Serebrov and J. Zmeskal, An apparatus for the investigation of solid  $D_2$  with respect to ultra-cold neutron sources, *Nuc. Instr. Meth. Phys. Res. A* **533** (2004), 491–504. doi:10.1016/j.nima.2004.06.157.
- [6] F.G. Brickwedde and R.B. Scott, The difference in vapor pressures of ortho and para deuterium, *J. Chem. Phys.* **3** (1935), 653. doi:10.1063/1.1749571.
- [7] J.C. Cook, J.G. Barker, J.M. Rowe, R.E. Williams, C. Gagnon, R.M. Lindstrom, R.M. Ibberson and D.A. Neumann, Experimental characterization of the advanced liquid hydrogen cold neutron source spectrum of the NBSR reactor at the NIST center for neutron research, *Nuc. Instr. Meth. Phys. Res. A* **792** (2015), 15–27. doi:10.1016/j.nima.2015.04.037.
- [8] S. Döge and J. Hingerl, A hydrogen leak-tight, transparent cryogenic sample container for ultra-cold neutron transmission measurements, *Rev. Sci. Instr.* **89** (2018), 033903. doi:10.1063/1.4996296.
- [9] W. Gaubatz and K. Gobrecht, The FRM-II cold neutron source, *Physica B: Cond. Mat.* **276** (2000), 104–105. doi:10.1016/S0921-4526(99)01260-0.
- [10] B.Y. Gorodilov, I.N. Krupskii, V.G. Manzhelii and O.A. Korolyuk, Thermal conductivity of ortho-para solutions of solid deuterium, *Fizika Nizkikh Temperatur* **7** (1981), 424–428, <http://fnt.ilt.kharkov.ua/main.php?page=10>.

- [11] T.M. Ito, E.R. Adamek, N.B. Callahan, J.H. Choi, S.M. Clayton, C. Cude-Woods, S. Currie, X. Ding, D.E. Fellers, P. Geltenbort, S.K. Lamoreaux, C.-Y. Liu, S. MacDonald, M. Makela, C.L. Morris, R.W. Pattie Jr., J.C. Ramsey, D.J. Salvat, A. Saunders, E.I. Sharapov, S. Sjue, A.P. Sprow, Z. Tang, H.L. Weaver, W. Wei and A.R. Young, Performance of the upgraded ultracold neutron source at Los Alamos National Laboratory and its implication for a possible neutron electric dipole moment experiment, *Phys. Rev. C* **97** (2018), 012501. doi:10.1103/PhysRevC.97.012501.
- [12] J. Karch, Y. Sobolev, M. Beck, K. Eberhardt, G. Hampel, W. Heil, R. Kieser, T. Reich, N. Trautmann and M. Ziegner, Performance of the solid deuterium ultra-cold neutron source at the pulsed reactor TRIGA Mainz, *European Phys. J. A* **50** (2014), 1–11. doi:10.1140/epja/i2014-14078-9.
- [13] M. Kasprzak, Thermal up-scattering of very cold and ultra-cold neutrons in solid deuterium, 2004, arXiv preprint, [arXiv:nucl-ex/0407022](https://arxiv.org/abs/nucl-ex/0407022).
- [14] E. Korobkina, Solid deuterium annealing, YouTube, 2018, <https://www.youtube.com/watch?v=LILgNyEeGjo>.
- [15] E. Korobkina, G. Medlin, B. Wehring, A.I. Hawari, P.R. Huffman, A.R. Young, B. Beaumont and G. Palmquist, Ultracold neutron source at the PULSTAR reactor: Engineering design and cryogenic testing, *Nuc. Instr. Meth. Phys. Res. A* **767** (2014), 169–175. doi:10.1016/j.nima.2014.08.016.
- [16] O.A. Korolyuk, B.Y. Gorodilov, A.I. Krivchikov and V.V. Dudkin, The role of normal processes in the thermal conductivity of solid deuterium, *Low Temp. Phys.* **26** (2000), 235. doi:10.1063/1.593891.
- [17] I.N. Krupskij, A.I. Prokhvatilov and G.N. Shcherbakov, Lattice parameters and thermal expansion of solid ortho-deuterium, *Fizika Nizkikh Temperatur* **10** (1984), 5–12, <http://fnt.ilt.kharkov.ua/main.php?page=10>.
- [18] T. Lauer, Investigation of a superthermal ultracold neutron source based on a solid deuterium converter for the TRIGA Mainz reactor, Dissertation, 2010.
- [19] C.-Y. Liu, A.R. Young and S.K. Lamoreaux, Ultracold neutron upscattering rates in a molecular deuterium crystal, *Phys. Rev. B* **62** (2000), R3581. doi:10.1103/PhysRevB.62.R3581.
- [20] G. Medlin, PhD thesis, <https://repository.lib.ncsu.edu/handle/1840.20/33644>.
- [21] A.R. Mueller, Characterization of solid deuterium as a source material for ultracold neutrons (UCN) and development of a detector concept for the detection of protons from neutron decay, Dissertation, TU Muenchen (2008).
- [22] Y.N. Pokotilovski, UCN transport simulation in solid deuterium crystals, *Nuc. Instr. Meth. Phys. Res. A* **675** (2012), 29–33. doi:10.1016/j.nima.2012.01.070.
- [23] V.F. Sears, Neutron scattering lengths and cross sections, *Neutron News* **3** (1992), 26–37. doi:10.1080/10448639208218770.
- [24] A. Serebrov, V. Mityukhlyayev, A. Zakharov, A. Kharitonov, V. Shustov, V. Kuz'minov, M. Lasakov, R. Tal'daev, A. Aldushchenkov, V. Varlamov, A. Vasil'ev, M. Sazhin, G. Greene, T. Bowles, R. Hill, S. Seestrom and P. Geltenbort, Studies of a solid-deuterium source for ultra-cold neutrons, *Nuc. Instr. Meth. Phys. Res. A* **440** (2000), 658–665. doi:10.1016/S0168-9002(99)01058-X.
- [25] A.P. Serebrov, Fundamental interactions involving neutrons and neutrinos: reactor-based studies led by Petersburg Nuclear Physics Institute (National Research Centre 'Kurchatov Institute') [PNPI (NRC KI)], *Phys.-Usp.* **58** (2015), 1074. doi:10.3367/UFNe.0185.201511c.1179.
- [26] I.F. Silvera, The solid molecular hydrogens in the condensed phase: Fundamentals and static properties, *Rev. Mod. Phys.* **52** (1980), 393. doi:10.1103/RevModPhys.52.393.
- [27] Y. Sobolev, Status of the UCN sources at the TRIGA Mainz reactor, 8th UCN workshop, PNPI, 2011, <http://cns.pnpi.spb.ru/ucn/articles/Sobolev.pdf>.
- [28] M. Sohaili, J. Klier and P. Leiderer, Triple-point wetting of molecular hydrogen isotopes, *J. Phys.: Cond. Mat.* **17** (2005), S415. doi:10.1088/0953-8984/17/9/009.
- [29] P.C. Souers, C.K. Briggs, J.W. Pyper and R.T. Tsugawa, Hydrogen vapor pressures from 4 to 30 K: A review, DOE Report, California Univ., Livermore (USA). Lawrence Livermore Lab., USA, 1977. doi:10.2172/7110677.
- [30] F. Weinhaus, H. Meyer, S.M. Myers and A.B. Harris, Nuclear-spin relaxation in the rotating frame in solid D<sub>2</sub>, *Phys. Rev. B* **7** (1973), 2960. doi:10.1103/PhysRevB.7.2960.
- [31] S. Wlokka et al., The ultra-cold neutron laboratory at the FRM II, Technical report, Verhandlungen der Deutschen Physikalischen Gesellschaft, 2015.
- [32] Z.-C. Yu, S.S. Malik and R. Golub, A thin film source of ultra-cold neutrons, *Zeitschrift für Physik B Cond. Mat.* **62** (1986), 137–142. doi:10.1007/BF01323423.